GEOFLUIDS

Geofluids (2011) **11**, 48–56 doi: 10.1111/j.1468-8123.2010.00305.x

Oscillatory zoning and trace element incorporation in hydrothermal minerals: insights from calcite growth experiments

SHAUN L.L. BARKER* AND STEPHEN F. COX

Research School of Earth Sciences, The Australian National University, Canberra, ACT, Australia

ABSTRACT

Oscillatory zoning and fine-scale variations in trace element chemistry are commonly observed in hydrothermal minerals. It has been suggested that fine-scale chemical variations are caused by extrinsic changes in the parent hydrothermal system, such as varying fluid composition, pressure or temperature, as well as changes in mineral growth rate. In this study, LA–ICP–MS (laser ablation, inductively coupled plasma mass spectrometer) analyses were carried out on calcite crystals grown in Ca–NH_3–Cl solutions doped with rare earth elements (REE). The variety of crystal morphologies observed (euhedral to acicular), likely relate to variations in trace element abundance and calcite supersaturation state. Crystals display oscillatory and sector zoning, with significant variations in REE concentrations among zones. Cyclic variations in REE concentrations (exceeding 10-fold) occur over distances of <1 mm along the growth direction of acicular calcite crystals. In general, trace element concentrations decrease during progressive crystal growth, implying that the concentration of trace and REEs within crystals reflects the overall composition of the growth solution. However, bulk changes in crystal composition are modulated by fine-scale (<1 mm) variations, which are inferred to be caused by growth-rate-controlled incorporation of trace elements. These results have important implications for using hydrothermal minerals to infer fluctuations in fluid compositions in ancient, exhumed hydrothermal systems.

Key words: calcite, hydrothermal, experiment, zoning, oscillatory

Received 24 August 2009; accepted 6 July 2010

Corresponding author: Shaun L. L. Barker, Research School of Earth Sciences, The Australian National University, Canberra, ACT 0200, Australia.
Email: sbarker@eos.ubc.ca. Tel: +1 (604) 822 1874. Fax: +1 (604) 822 6088.
*Present address: Department of Earth and Ocean Sciences, University of British Columbia, 6339 Stores Rd, Vancouver, BC V6T1Z4, Canada.

Geofluids (2011) **11**, 48–56

INTRODUCTION

Veins composed of hydrothermal minerals contain the integrated record of hot fluids migrating through the Earth's crust. Fluid migration leads to various mineral reactions, and the precipitation of hydrothermal minerals. Zoned minerals, deposited from hydrothermal solution, may provide semi-continuous records of hydrothermal fluid chemistry (e.g. Rye & Bradbury 1988; Jamtveit & Hervig 1994; Cline 2001; Elburg *et al.* 2002; Rusk & Reed 2002; Rusk *et al.* 2008, along with numerous other examples). These records are useful to determine how hydrothermal systems evolved, and are of particular interest in ore-forming hydrothermal systems, where hydrothermal minerals may record key processes of metal precipitation. Studies of hydrothermal mineral composition require that the hydrothermal mineral growth mechanism is well constrained, i.e. the relative timing of mineral precipitation is known. In addition, an understanding of the variation in trace element and isotopic compositions of minerals precipitated at different locations at the same time (i.e. compositional zoning) is required.

Previous studies have demonstrated that various processes affect the chemical and isotopic composition of hydrothermal minerals, including changes in fluid source and fluid flow pathways (e.g. Rye & Bradbury 1988;

Wogelius *et al.* 1997; Cline 2001; Elburg *et al.* 2002; Rusk & Reed 2002; Barker *et al.* 2006; Rusk *et al.* 2006; Allan & Yardley 2007; Cox 2007). Zoned hydrothermal minerals are common, and include sulphide (e.g. pyrite), silicate (e.g. quartz) and carbonate (e.g. calcite, dolomite) minerals. Different growth zones in sulphide minerals have been demonstrated to be caused by several stages of sulphide precipitation, during several separate hydrothermal events (e.g. pyrite in Carlin-type gold-bearing hydrothermal systems; Cline & Hofstra 2000; Cline 2001; Barker *et al.* 2009), and to crystallographic controls on the differential uptake of trace elements into sulphide during a single hydrothermal event (e.g. Chouinard *et al.* 2005). Variations in trace element concentrations and textures in hydrothermal quartz veins have been related to changes in temperature, pH, oxygen fugacity and fluid source (Flem *et al.* 2002; Monecke *et al.* 2002; Mueller *et al.* 2003; Rusk *et al.* 2006, 2008). Concentric zoning of trace elements in natural carbonate cements has been widely reported, and is commonly interpreted to be caused by fluctuations in bulk fluid composition (see review of Shore & Fowler 1996).

In addition to geological controls on the composition of hydrothermal minerals, various disequilibrium and non-linear processes further modulate the isotopic and trace element composition of hydrothermal minerals (Ortoleva *et al.* 1987; Dickson 1991; Onasch & Vennemann 1995; Jourdan *et al.* 2006; Allan & Yardley 2007; van Hinsberg & Marschall 2007). Several crystal growth studies (e.g. Reeder & Grams 1987; Paquette & Reeder 1990, 1995; Reeder *et al.* 1990; Prieto *et al.* 1997) have demonstrated that zoned crystals may be precipitated from solutions that have approximately constant composition throughout crystal growth. These studies show that considerable stable isotope and trace and minor element variability occur within and between single minerals precipitated at equivalent times. Thus, considerable caution is required when interpreting variations in trace element concentrations within hydrothermal minerals.

Changes in rare earth element (REE) concentrations and patterns are of particular interest in hydrothermal minerals, as they likely respond to changes in absolute REE concentrations in solution, fluid oxidation state and changes in the types and concentrations of REE-complexing species (Bau 1991; Bau & Moller 1992). In this study, we document the morphology, internal zoning and REE compositions of synthetic calcite crystals grown in REE-doped solutions. Laser ablation, inductively coupled plasma mass spectrometry (LA–ICP–MS) is used to measure REE concentrations variations in crystals grown from solutions of approximately constant composition. These results have implications for the interpretation of changes in trace and REE concentrations in natural hydrothermal minerals.

METHODS

Calcite crystals were grown using the method of Gruzensky 1967; where NH_3 and CO_2 gases sublime from ammonium carbonate, and diffuse into an aqueous solution of calcium and ammonium chloride, causing calcite supersaturation and precipitation. Approximately 850 ml of MilliQ water (>18 MΩ resistance) was placed into four 1 l LDPE Nalgene-Nunc brand bottles. Into this, sufficient $CaCl_2$ and NH_4Cl (analytical reagent grade, 99.9% pure) were added to create a solution with calculated Ca^{2+}concentrations of approximately 0.02 and 0.17 mol l^{-1} (Table 1). Into these solutions, a mixed REE spike (La, Ce, Nd, Sm, Eu, Gd, Dy, Er, Yb, Lu), created from pure REE metals dissolved and stabilized in HNO_3, was added to create solutions with known concentrations of approximately 10 and 100 ppb (parts per billion) REEs (see Table 1). Mg, Fe, Sr and Mn were not added intentionally to solutions, and are likely due to contamination of the reagent grade $CaCl_2$ starting solution.

Initial solution pH was low, as a result of the acidic REE spike. Starting pH values in the 100-ppb solutions were 1.9–2, whereas initial pH values in the 10-ppb solutions were 5 and 6.3. Bottles were immersed in a temperature-controlled water bath, at a constant temperature of 30°C. Over several days, solution pH rose, and stabilized at values of 7.4–7.8. Calcite precipitation began within a few days of pH stabilization, as carbon dioxide diffused into the solution. After 3 months, calcite crystals were recovered from solution by placing the bottles in an ultrasonic bath for 15 min, and passing the solutions through a filter paper. Significant fine-grained calcite 'scale' remained inside the bottles. The growth of calcite in all solutions was confirmed by XRD analysis. Crystal morphology was examined using light and scanning electron microscopy (SEM). Recovered crystals were mounted in epoxy and polished to expose the core of crystals and examined using

Table 1 Starting compositions of major ion and REE concentrations in different solutions.

Chemical Species	Solution 1	Solution 2	Solution 3	Solution 4
Ca^{2+} (mol l^{-1})	0.168	0.170	0.016	0.017
NH_4^+ (mol l^{-1})	0.663	0.609	0.482	0.427
Cl^- (mol l^{-1})	0.998	0.949	0.515	0.461
La (ppb)	94	9.4	97	9.6
Ce (ppb)	100	10.0	103	10.2
Nd (ppb)	93	9.4	96	9.6
Sm (ppb)	94	9.5	97	9.6
Eu (ppb)	104	10.4	107	10.6
Gd (ppb)	99	9.9	102	10.1
Dy (ppb)	94	9.4	97	9.6
Er (ppb)	91	9.2	94	9.3
Yb (ppb)	92	9.2	95	9.4
Lu (ppb)	89	8.9	92	9.1

both SEM-based and optical cathodoluminesence (CL) to reveal internal zoning.

The distribution and concentrations of Mg, Mn, Sr, Fe and REEs were determined by LA–ICP–MS. Samples were analysed using a pulsed ArF Excimer laser (λ = 193 nm) and a quadrupole ICP–MS (Agilent 7500s). The sample was moved at a steady speed (approximately 30 μm sec^{-1}) beneath the laser beam, facilitating *in situ*, high-spatial resolution, continuous data collection (Eggins *et al.* 1998). Samples were precleaned with ethanol, and the area chosen for analysis was 'laser cleaned' by a laser ablation prescan. Two parallel laser line scans were carried out along one polished needle. In addition, multiple spot analyses were made on other selected crystals. Major and trace elements (^{24}Mg, ^{43}Ca, ^{44}Ca, ^{45}Sc, ^{49}Mn, ^{57}Fe, ^{85}Rb, ^{88}Sr, ^{89}Y, ^{138}Ba, ^{139}La, ^{140}Ce, ^{141}Pr, ^{146}Nd, ^{147}Sm, ^{153}Eu, ^{158}Gd, ^{163}Dy, ^{166}Er, ^{174}Yb) were simultaneously profiled during laser sampling by repeated, rapid sequential peak hopping, with a mass spectrometer cycle time of 0.37 sec. Data reduction followed established protocols for time-resolved analysis (Longerich *et al.* 1996). High-spatial resolution was achieved by using 20-μm spots at 10 laser pulses per second with a moderately low laser fluence (5 J cm^{-2}), and by minimizing mean particulate residence times in the ablation cell volume following each laser pulse (Eggins *et al.* 1998). Internal standardization was carried out using ^{43}Ca. During initial data reduction, data are binned into 1-sec intervals, giving a spatial resolution of 30 μm. The NIST 612 glass standard was used for calibration, using the values of Pearce *et al.* (1997).

During laser ablation spot analysis, individual growth zones were targeted on the basis of CL images. However, individual growth zones identified by CL at the surface do not necessarily extend in the third dimension. Thus, analyses conducted on equivalent growth zones on crystals may be influenced by varying morphology in the third dimension, and this possibility must be taken into account during interpretation of laser ablation data. Such changes in morphology would also be present in natural crystals.

RESULTS

Sample description

Solutions 2 (high Ca, low REE) and 4 (low Ca, low REE; see Table 1) grew a mixture of fine-grained crystal aggregates, and stubby to equant calcite crystals. These crystals display both sector and oscillatory zoning under CL. Crystals grown from solution 1 (high Ca, high REE) show a 'tulip' morphology, with a narrow, 'stalk' base and bulbous terminus with well-developed crystal faces (Fig. 1A). In surfaces cut parallel to the long axis of the crystal, CL reveals bright, patchy cores at the crystal bases and poorly luminescent calcite at the crystal edges. In surfaces cut perpendicular to the long axis of the crystal, CL imaging reveals (Fig. 1A) bright cores with oscillatory zoning (zones approximately 20 μm wide) and sector-zoned overgrowths.

Crystals grown from solution 3 (low Ca, high REE) have a markedly different (acicular) morphology to the other crystals. Crystals are up to several millimetres in length and <0.5 mm wide (Fig. 1B). SEM images reveal that the needles are formed from a network of bladed subcrystals with a scalenohedral morphology (Fig. 1C). Examination of the needles in thin section reveals that each needle is composed of one continuous calcite crystal. Cathodoluminescence imaging of calcite needles reveals thin bands approximately 20–40 μm thick, perpendicular to the long axis of the crystal (Fig. 1D).

Figure 2 shows the results of a laser ablation line profile along a polished needle grown in solution 3 (full results from the two adjacent traverses may be found in the Data S1). Strontium and Mg were not added into the REE spike, and are presumably due to contamination in the $CaCl_2$ powder from which solutions were prepared. Magnesium concentrations average 35 ppm (parts per million) in one traverse, and 50 ppm in the other traverse. Strontium concentrations lie between 20 and 40 ppm, and are relatively well correlated between traverses (r^2 = 0.42). In addition, Mn (r^2 = 0.28) and Ba (r^2 = 0.26) are relatively well correlated between traverses, whereas Fe (r^2 = 0.02) and Mg (r^2 = 0.03) are poorly correlated between traverses. REE concentrations are high (tens to hundreds of ppm). Lanthanum and Yb concentrations (Fig. 2) vary significantly over distances of <0.5 mm, with changes in REE concentrations highly correlated within each traverse. In addition, changes in REE are well correlated between traverses (see Data S1). It is noted that changes in trace element concentrations along line profiles carried out on fibres vary substantially more (relative standard deviation >50%) than line profiles made along NIST 612 glass standard (relative standard deviation of 2–3%). Thus, the trace element variations observed along crystals are not likely to be analytical artefacts.

Figures 3 and 4 show cathodoluminescence zoning of latitudinal and longitudinal slices (respectively) cut through elongate crystals from solution 1, as well as REE patterns from selected analyses (determined by LA–ICP–MS). These crystals are very similar in shape to the crystal from solution 1 shown in Fig. 1a. REE concentrations are the highest at the core of crystals (coincident with highest CL intensity) and generally become lower towards the outside of the crystals. This is consistent with preferential uptake of REE from solution, and gradual drawdown of REE concentrations in the solution. At the base of the crystal (where growth began), REE concentrations are high [with middle rare earth elements (MREE) depletion]. Near the top of the crystal (in the region of euhedral crystal growth), REE patterns become flatter, and REE

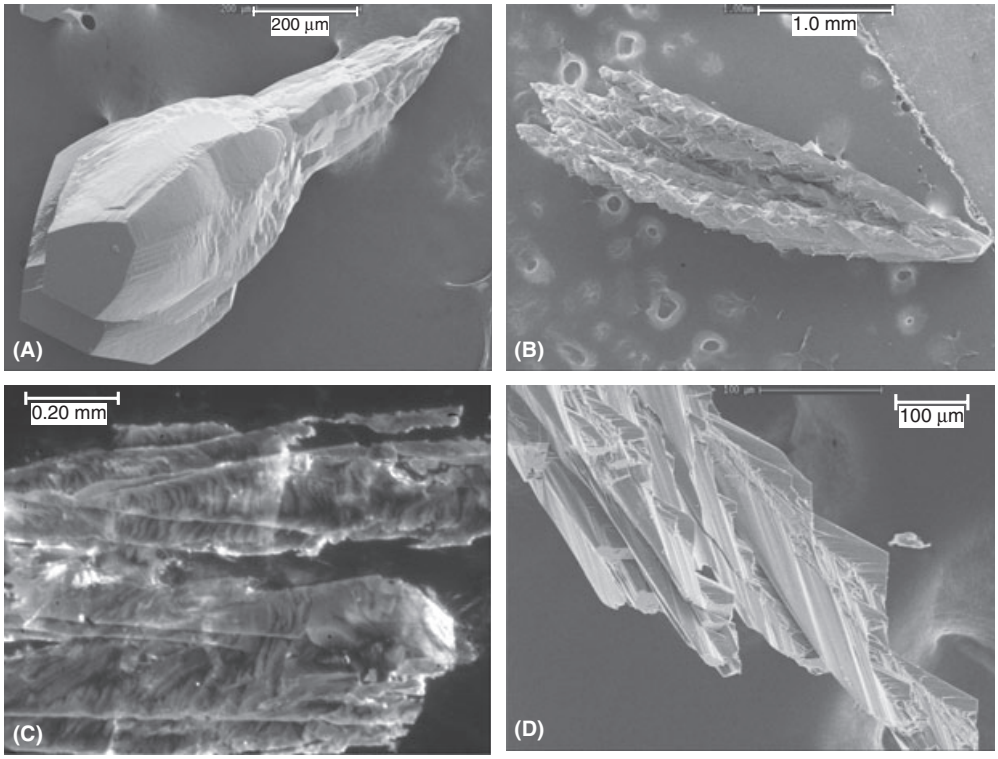

Fig. 1. (A) SEM secondary electron (SE) photomicrograph of elongate euhedral 'tulip' crystals grown from high Ca, high REE solution (solution 1). Note elongate, tube-like bases to crystals, with crystal tops defined by well-developed rhombohedral faces. (B) SEM SE photomicrograph of acicular calcite crystal grown from the low Ca, high REE solution (solution 3). (C) SEM SE photomicrograph showing the enlargement of termination of an acicular calcite crystal grown in solution 3. (D) CL photomicrograph of section of acicular calcite crystal from solution 3. Note fine-scale banding perpendicular to long-axis of crystal.

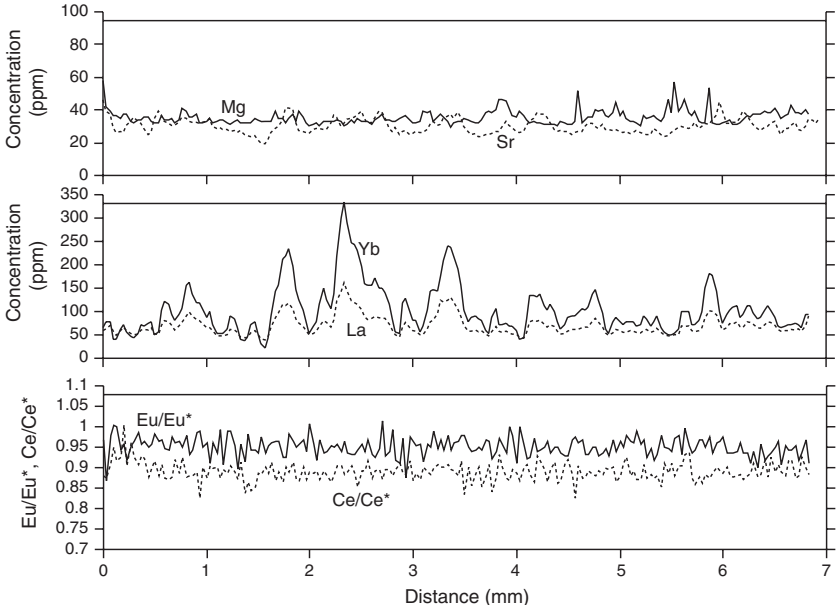

Fig. 2. Results of a laser ablation ICP–MS line scan along the long axis of a polished acicular calcite needle from solution 3. Magnesium, Sr, La and Yb concentrations (parts per million) are shown, as well as Eu/Eu* and Ce/Ce* ratios. Note significant concentration variations over scales of <0.5 mm. Spatial resolution is approximately 30 μm.

concentrations decrease. Calcite with brighter luminescence is coincident with higher REE and Sr concentrations. The transition from highly luminescent calcite to poorly luminescent calcite is coincident with the change in crystal morphology from the narrow 'stalk-like' base to the bulbous head (Fig. 1a).

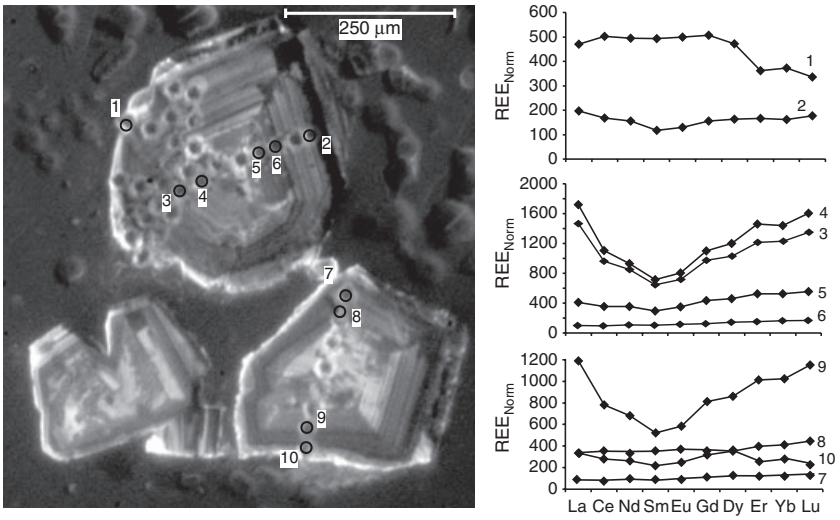

Fig. 3. Cathodoluminescence photomicrograph of latitudinal sections through the top of three elongate calcite crystals from solution 1. Circles are the location of individual laser ablation ICP–MS analyses. Numbers refer to the analysis numbers shown in the adjacent graphs. Analyses 1 and 2 are from different crystal faces at equivalent growth stages. Rare earth element concentrations are normalized to the REE concentrations in the starting solution (see Table 1).

DISCUSSION

In the following section, we discuss the implication of the results outlined above for the interpretation of trace and REE variations in natural hydrothermal minerals. The REE concentrations reported within the calcite precipitated in this study (for example, Ce concentrations within the acicular calcite needles vary between 3 and 130 ppm, with a median value of 36 ppm) are similar, or somewhat higher than concentrations reported in hydrothermal calcite veins. In natural calcite veins, Barker (2007) reported Ce concentrations between <1 and 100 ppm. Similarly, Bau & Moller (1992), Hecht *et al.* (1999) and Uysal *et al.* (2007) report Ce concentrations between <1 and 50 ppm for fracture-filling carbonate minerals. However, heavy REE concentrations in the calcite precipitated in this study (e.g. Yb) are significantly elevated above concentrations typically reported for natural, fracture-filling carbonate minerals (e.g. Bau & Moller 1992; Hecht *et al.* 1999; Uysal *et al.* 2007). These high heavy rare earth elements (HREE) concentrations likely reflect the elevated concentrations of HREE present in the starting solution. Partition coefficients for all REEs estimated for this study ($C_{solid}/C_{solution}$) between fluid and calcite are on the order of approximately 10^2 to approximately 10^3, and are broadly compatible with the partition coefficients determined for REEs by Zhong & Mucci (1995). However, REE patterns observed [MREE depleted, both light rare earth elements (LREE) and HREE enriched patterns] are considerably different from patterns observed by Zhong & Mucci (1995), which may be related to different experimental conditions.

The growth of calcite needles in solution 3 proved to be serendipitous, as it allows changes in calcite chemistry over time to be examined more easily than in the rhombohedral crystals, as the relative timing of crystal growth can be more easily interpreted. Similarly, in natural hydrothermal veins, antitaxial and syntaxial fibrous veins that grow progressively (Durney & Ramsay 1973; Oliver & Bons 2001) may be used to trace the evolution of a hydrothermal system over time (Barker *et al.* 2006). Two points of interest raised by these results are:

(1) Trace element concentrations can vary by an order of magnitude over distances of approximately 200 μm in the calcite needles.
(2) No systematic variations in cerium or europium anomalies were noted during the growth of the calcite needles.

The deviation of normalized Ce and Eu values from those anticipated in a mineral is known as a Ce or Eu anomaly. This is expressed as Ce/Ce*, or Eu/Eu*, where Ce* and Eu* are the predicted normalized values, based on the normalized values of the adjacent REEs (Towell *et al.* 1965). Cerium and Eu anomalies in hydrothermal minerals have been used to infer variations in fluid-rock reaction, fluid source and fluid oxidation state (e.g. Bau & Moller 1992; Brugger *et al.* 2006). Europium (Eu/Eu*) and cerium (Ce/Ce*) anomalies along the long axis of a calcite needle are shown in Fig. 2. Values for Eu/Eu* are not different at the 2σ level between the adjacent traverses (0.84 ± 0.1 and 0.95 ± 0.05). Average values for Ce/Ce* are identical for the two traverses.

Calcite near the edges of crystals generally had low REE concentrations, which is inferred to be due to drawdown of REE from the fluid reservoir. Due to the inadvertent discarding of the growth solutions, REE concentrations were not measured at the end of the growth experiments, making this impossible to verify.

Rare earth element patterns show some variation between different sector zones, with variable MREE depletion. However, patterns remained relatively flat showing no significant LREE enrichment or HREE enrichment. In addition, no significant changes in Eu or Ce anomalies

were measured within or between crystals. Wood (1990) determined that at low-temperatures (25°C), trivalent REE species will dominate. Thus, in the experiments described in this study, the generation of REE anomalies due to changes in oxidation state would not be anticipated. Changes in Ce and Eu anomalies during the growth of hydrothermal vein minerals are likely to indicate that an extrinsic factor (fluid mixing, fluid–rock reaction) has affected the composition or oxidation state of the hydrothermal fluid. In contrast, REE patterns may be somewhat influenced by crystallographic affects, with results from this study indicating that the MREE concentrations are more variable than the light and heavy REE, with flat to concave REE patterns measured within the same crystal (Fig. 3).

The fine-scale variations in REE concentrations observed in these synthetic calcite needles are similar (in distance and concentration change) to the variations in trace and REE concentrations determined in natural hydrothermal carbonate veins by Wogelius *et al.* (1997), Elburg *et al.* (2002) and Barker *et al.* (2006). The spatial scale of the trace element concentrations changes appears similar to the scale of the banding observed in the laboratory-grown acicular calcite crystals (Fig. 1d). Notable is that trace element concentrations can vary by up to an order of magnitude over several hundred microns. Furthermore, trace element concentrations fluctuate with distance (equivalent to fluctuations in time). This is an important observation, as it suggests that trace element concentrations alone cannot be used to make inferences about extrinsic chemical changes in the fluid from which calcite precipitated, but additional information, such as stable or radiogenic isotope data, is required.

This set of exploratory experiments reveals new information on REE zoning within calcite. In general: (i) calcite inferred to have precipitated at the start of crystal growth has higher REE concentrations, and MREE depleted patterns; (ii) calcite precipitated towards the end of crystal growth has lower REE concentrations and flat to LREE enriched patterns; and (iii) oscillatory and sector zoning is developed within calcite crystals. These observations have important implications for natural hydrothermal carbonate minerals. In general, a monotonic change in REE concentrations, patterns, or Ce and Eu anomalies would reflect a geological process of some kind. However, oscillatory trace element concentration zoning preserved within hydrothermal minerals may not reflect any particular geological process (such as crack-seal growth of hydrothermal minerals, or variable supply of fluid due to changes in the permeability structure of surrounding rocks).

Growth-rate control on trace element uptake in natural veins

In the analyses conducted along the acicular crystals, different trace elements show contrasting behaviour in adjacent traverses along the same calcite needle (Fig. 2). As described above, Sr concentrations correlate well between traverses on the same crystal, whereas Mg concentrations are poorly correlated. This is similar to the behaviour for different trace elements in vein calcite noted by Barker *et al.* (2006), which implies that there is a fundamental difference in behaviour between different trace elements during their uptake into the calcite crystal lattice. The lack of correlation between changes in Mg and Sr concentrations rules out the inhibition mechanism of Wang & Merino (1992), which should affect all divalent cations in a similar manner.

Fine-scale variations in trace element concentrations in calcite may be explained by the growth entrapment model of Watson (1996, 2004), which suggests that the concentration of a trace element in a growing crystal is controlled by the concentration of that element in the 'near-surface' region of the growing crystal, and competition between crystal growth (trapping surface enriched elements) and ion migration in the near-surface region (which attempts to rid the crystal lattice of impurities). Therefore, the spacing and amplitude of compositional zones could provide quantitative information about the precipitation rate of material in hydrothermal veins, if growth-rate-controlled fluctuations could be separated from the extrinsic affects of geological controls.

Watson (2004) used the data of Lorens (1981) and Tesoriero & Pankow (1996) to estimate partition coefficients between calcite crystals and parent solutions at different calcite growth rates. Strontium and Ba show higher partition coefficients at higher growth rates, whereas Mn shows lower partition coefficients at higher growth rates. In the calcite needles, Sr and Mn concentrations show a weak negative correlation ($r^2 = -0.30$) and Sr and Ba concentrations show a weak positive correlation ($r^2 = +0.43$), consistent with the incorporation of these trace elements being somewhat controlled by crystal growth rate. In addition, the base of the 'tulip' crystals (Fig. 4) has higher concentrations of Sr, and lower concentrations of Mn, consistent with faster growth rates at the base of the 'tulip stem' and slower growth rates in the 'tulip bulb'.

It is suggested that calcite that precipitated at faster rates would preserve more significant compositional zoning, because variations in the near-surface region of the crystal would be captured by the more rapidly growing crystal (Watson 2004). Contrastingly, calcite precipitated more slowly would have less prevalent compositional zoning, because there is more time for elements in solution to diffuse through the surface layer and reach equilibrium with the crystal lattice. Gabitov & Watson (2006) suggested that crystal growth rates slower than 0.5 mm year^{-1} are required to reach equilibrium partitioning of Sr between a growing calcite crystal and fluid at 25°C. Therefore, calcite crystals forming in a hydrothermal vein would need to

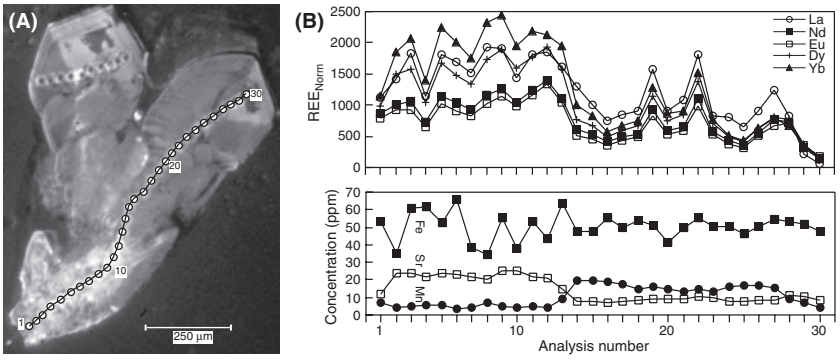

Fig. 4. (A) Cathodoluminescence photomicrograph along the long axis of an elongate calcite crystal grown in solution 1. Circles are the location of individual laser ablation ICP–MS analyses. Numbers refer to the analysis numbers shown in (B). (B) Graphs showing REE (REE concentrations are normalized to the REE concentrations in the starting solution, see Table 1), Sr, Mn and Fe concentrations along the length of the crystal for analysis spots marked on crystals.

grow at a rate of more than 0.5 mm per year to capture fine-scale variations in Sr concentrations (assuming that there were no external controls on Sr supply, or significant changes in temperature or pressure that might affect Sr uptake). Indeed, faster growth rates would probably be required to preserve compositional variations, as trace element diffusion rates will be faster at higher temperatures.

Hydrothermal vein textures

An important result from these experiments is the variation in crystal morphology described in calcite, which grew in different composition solutions. Among the four solutions, those with higher REE concentrations grew elongate and needle-like crystals, whereas solutions with lower REE concentrations grew equant to stubby crystals with rhombohedral and prism faces. Previous workers have suggested that a variety of factors influence carbonate mineral crystal habits. Given & Wilkinson (1985) suggested that carbonate crystal morphologies are controlled by the rate at which growth nutrients are supplied. Calcite growth experiments by Gonzalez *et al.* (1991) found that at low supersaturation states, crystal habits are limited to those with shallow to steep rhombohedral forms, whereas with increasing supersaturation, scalenohedrons, extremely steep rhombohedrons, pinacoids and hexagonal prisms are developed. In addition, Fernandez-Diaz *et al.* (1996) determined that Mg-calcite crystal morphology varied as a function of calcite supersaturation and (Mg^{2+}). More recently, Pastero *et al.* (2004) carried out a series of calcite growth experiments from solutions doped with Li, and found that crystal morphology varied as a function of calcite supersaturation state and $(Li^{+})/(Ca^{2+})$. In comparison, Garcia-Ruiz (1998) suggested that the morphology of experimentally synthesized barium and strontium carbonates varied primarily as a function of pH. In the experiments carried out in this study, we consider it likely that the crystal morphology in these experiments is controlled both by the calcite supersaturation state and $(REE^{3+})/(Ca^{2+})$ ratio.

Crystal morphology in hydrothermal veins (influencing vein texture) is commonly interpreted in terms of variable rates of vein opening and mineral precipitation rate (see review of Oliver & Bons 2001). However, vein textures may also be critically dependent on which crystal habits dominate (cf. Dickson 1983). During growth of hydrothermal minerals into an open, fluid-filled space, vein textures are likely very sensitive to calcite supersaturation state, and the concentration of rare earth and other trace elements. Fluids with higher trace element concentrations would be predicted to produce fibrous intergrowths, with more equigranular textures associated with rhombohedral forms at lower trace element concentrations.

CONCLUSIONS

Moderate-sized (<1–5 mm) synthetic calcite crystals were grown from solutions with variable (Ca^{2+}) and variable $(REE^{3+})/(Ca^{2+})$. Needle-like and elongate crystals grew from solutions with higher concentrations of $(REE^{3+})/(Ca^{2+})$, whereas solutions with lower $(REE^{3+})/(Ca^{2+})$ precipitated calcite crystals dominated by rhombohedral and prism faces. Changes in crystal morphology are likely caused by variable calcite supersaturation state and $(REE^{3+})/(Ca^{2+})$. The influence of solution chemistry on crystal morphology has important implications for the interpretation of hydrothermal vein textures. REE concentrations decrease from crystal cores to rims, indicating that REEs were progressively taken up from solution (leading to depleted REE concentrations in solution). High-spatial resolution LA–ICP–MS analyses of synthetic calcite crystals demonstrate significant fluctuations in Mg, Fe, Sr and REE concentrations over distances of <200 μm in the inferred growth directions of crystals. These analyses indicate that fluctuations in the trace element content of natural carbonates cannot be interpreted strictly in terms of extrinsic changes in fluid chemistry. However, Eu/Eu* and Ce/Ce* anomalies do not appear to be as significantly influenced by compositional zoning, and may be a robust indicator of changes in bulk solution chemistry or oxidation state. Further experimental work, with integrated monitoring of crystal growth and solution chemistry, is needed to constrain variables such as REE speciation, crystal growth rates, and

links between changes in crystal morphology and solution chemistry.

ACKNOWLEDGEMENTS

D.C. 'Bear' McPhail is thanked for extremely useful discussions during this project. SLLB was in receipt of an Australian Postgraduate Award, and acknowledges RSES and the ANU for additional scholarship support. Harri Kokkonen helped with petrographic preparation. Sally Stowe at the ANU EMU assisted with SEM CL observations. Charlotte Allen and Chuck Magee provided assistance with LA–ICP–MS analyses. Paul Bons, Brian Rusk and an anonymous reviewer are thanked for reviews that improved this article, and Richard Worden is thanked for editorial guidance.

SUPPORTING INFORMATION

Additional supporting Information may be found in the online version of this article:

Data S1. Spreadsheets from the two parallel laser ablation line profiles carried out on a calcite needle grown in solution 3. Included are the raw data, as well as separate sheets showing the correlation and links between trace elements. All concentrations are given in parts per million (ppm).

Please note: Wiley-Blackwell are not responsible for the content or functionality of any supporting materials supplied by the authors. Any queries (other than missing material) should be directed to the corresponding author for the article.

REFERENCES

Allan M, Yardley B (2007) Tracking meteoric infiltration into a magmatic-hydrothermal system: a cathodoluminescence, oxygen isotope and trace element study of quartz from Mt. Leyshon, Australia. *Chemical Geology*, **240**, 343–60.

Barker S (2007) *Dynamics of fluid flow and fluid chemistry during crustal shortening.* PhD thesis, Research School of Earth Sciences, The Australian National University, Canberra.

Barker S, Cox S, Eggins S, Gagan M (2006) Microchemical evidence for episodic growth of antitaxial veins during fracture-controlled fluid flow. *Earth and Planetary Science Letters*, **250**, 331–44.

Barker S, Hickey K, Cline J, Dipple G, Kilburn M, Vaughan J, Longo A (2009) Uncloaking invisible gold: use of nanoSIMS to evaluate gold, trace elements and sulfur isotopes in pyrite from Carlin-type gold deposits. *Economic Geology and the Bulletin of the Society of Economic Geologists*, **104**, 897–904.

Bau M (1991) Rare-earth element mobility during hydrothermal and meta-morphic fluid-rock interaction and the significance of the oxidation state of europium. *Chemical Geology*, **93**, 219–30.

Bau M, Moller P (1992) Rare earth element fractionation in metamorphogenic hydrothermal calcite, magnesite and siderite. *Mineralogy and Petrology*, **45**, 231–46.

Brugger J, Etschmann B, Chu Y, Harland C, Vogt S, Ryan C, Jones H (2006) The oxidation state of europium in hydrothermal scheelite: in situ measurement by XANES spectroscopy. *The Canadian Mineralogist*, **44**, 1079–87.

Chouinard A, Paquette J, William-Jones A (2005) Crystallo-graphic controls on trace-element incorporation in auriferous pyrite from the Pascua epithermal high-sulfidation deposit, Chile-Argentina. *The Canadian Mineralogist*, **43**, 951–63.

Cline J (2001) Timing of gold and arsenic sulfide mineral deposition at the Getchell Carlin-type deposit, north-central Nevada. *Economic Geology and the Bulletin of the Society of Economic Geologists*, **97**, 75–89.

Cline J, Hofstra A (2000) Ore-fluid evolution at the Getchell Carlin-type gold deposit, Nevada, USA. *European Journal of Mineralogy*, **12**, 195–212.

Cox SF (2007) Structural and isotopic constraints on fluid flow regimes and fluid pathways during upper crustal deformation: an example from the Taemas area of the Lachlan Orogen, south-eastern Australia. *Journal of Geophysical Research*, **112**, B08208; doi: 10.1029/2006JB004734.

Dickson J (1983) Graphic modelling of crystal aggregates and its relevance to cement diagnosis. *Philosophical Transactions of the Royal Society of London Series A*, **309**, 465–502.

Dickson J (1991) Disequilibrium carbon and oxygen isotope variations in natural calcite. *Nature*, **353**, 842–4.

Durney D, Ramsay J (1973) Incremental strains measured by syntectonic crystal growths. In: *Gravity and Tectonics* (eds De Jong K, Scholten R), pp. 67–96. Wiley, New York, New York.

Eggins S, Kinsley L, Shelley J (1998) Deposition and element fractionation processes during atmospheric pressure laser sampling for analysis by ICP-MS. *Applied Surface Science*, **127-129**, 278–86.

Elburg M, Bons P, Foden J, Passchier C (2002) The origin of fibrous veins: constraints from geochemistry. In: *Deformation Mechanisms, Rheology and Tectonics: Current Status and Future Perspectives* (eds De Meer S, Drury M, De Bresser J, Pennock G), pp. 103–18, Vol. 200, Geological Society of London Special Publications. Geological Society of London, London.

Fernandez-Diaz L, Putnis A, Prieto M, Putnis CV (1996) The role of magnesium in the crystallization of calcite and aragonite in a porous medium. *Journal of Sedimentary Research*, **66**, 482–91.

Flem B, Larsen R, Grimstvedt A, Mansfeld J (2002) In situ analysis of trace elements in quartz by using laser ablation inductively coupled plasma mass spectrometry. *Chemical Geology*, **182**, 237–47.

Gabitov R, Watson E (2006) Partitioning of strontium between calcite and fluid. *Geochemistry Geophysics Geosystems*, **7**, Q11004; doi: 10.1029/2005GC0011216.

Garcia-Ruiz J (1998) Carbonate precipitation into alkaline silica-rich environments. *Geology*, **26**, 843–6.

Given R, Wilkinson B (1985) Kinetic control of morphology, composition, and mineralogy of abiotic sedimentary carbonates. *Journal of Sedimentary Petrology*, **55**, 109–19.

Gonzalez LA, Carpenter S, Lohmann K (1991) Inorganic calcite morphology: roles of fluid chemistry and fluid flow. *Journal of Sedimentary Petrology*, **62**, 382–99.

Gruzensky P (1967) Growth of calcite crystals. In: *Crystal Growth* (ed. Peiser H), pp. 365–7. Pergamon Press, Oxford.

Hecht L, Freiberger R, Gilg H, Grundmann G, Kostitsyn Y (1999) Rare earth element and isotope (C, O, Sr) characteristics of hydrothermal carbonates; genetic implications for dolomite-hosted talc mineralization at Goepfersgruen (Fichtelgebirge, Germany). *Chemical Geology*, **155**, 115–30.

van Hinsberg V, Marschall H (2007) Boron isotope and light element sector zoning in tourmaline: implications for the formation of B-isotopic signatures. *Chemical Geology*, **238**, 141–8.

Jamtveit B, Hervig R (1994) Constraints on transport and kinetics in hydrothermal systems from zoned garnet crystals. *Science*, **263**, 505–8.

Jourdan A, Vennemann T, Mullis J, Ramseyer K (2006) Sector zoning of trace elements and oxygen isotopes in natural quartz crystals. *Geochimica et Cosmochimica Acta*, **70**, A298.

Longerich H, Jackson S, Gunter D (1996) Laser ablation inductively coupled plasma mass spectrometric transient signal data acquisition and analyte concentration calculation. *Journal of Analytical Atomic Spectrometry*, **11**, 899–904.

Lorens R (1981) Sr, Cd, Mn and Co distribution coefficients in calcite as a function of calcite precipitation rate. *Geochimica et Cosmochimica Acta*, **45**, 553–61.

Monecke T, Kempe U, Gotze J (2002) Genetic significance of the trace element content in metamorphic and hydrothermal quartz: a reconnaissance study. *Earth and Planetary Science Letters*, **202**, 709–24.

Mueller A, Wiedenbeck M, Van Den Kerkhof A, Kronz A, Simon K (2003) Trace elements in quartz – a combined electron microprobe, secondary ion mass spectrometry, laser-ablation ICP-MS, and cathodolumi-nescence study. *European Journal of Mineralogy*, **15**, 747–63.

Oliver N, Bons P (2001) Mechanisms of fluid flow and fluid-rock interaction in fossil metamorphic hydrothermal systems inferred from vein-wallrock patterns, geometry and microstructure. *Geofluids*, **1**, 137–62.

Onasch CM, Vennemann TW (1995) Disequilibrium partitioning of oxygen isotopes associated with sector zoning in quartz. *Geology*, **23**, 1103–6.

Ortoleva P, Merino E, Moore C, Chadam J (1987) Geochemical self-organization I; reaction-transport feedbacks and modeling approach. *American Journal of Science*, **287**, 979–1007.

Paquette J, Reeder R (1990) New type of compositional zoning in calcite: insights into crystal-growth mechanism. *Geology*, **18**, 1244–7.

Paquette J, Reeder R (1995) Relationship between surface structure, growth mechanism, and trace element incorporation in calcite. *Geochimica et Cosmochimica Acta*, **59**, 735–49.

Pastero L, Costa E, Bruno M, Rubbo M, Sgualdino G, Aquilano D (2004) Morphology of calcite (CaCO3) crystals growing from aqueous solutions in the presence of Li+ ions. Surface behaviour of the {0001} form. *Crystal Growth & Design*, **4**, 485–90.

Pearce N, Perkins W, Westgate J, Gorton M, Jackson S, Neal C, Chenery S (1997) A compilation of new and published major and trace element data for NIST SRM 610 and NIST SRM 612 glass reference materials. *Geostandards Newsletter*, **21**, 115–44.

Prieto M, Fernandez-Gonzalez A, Putnis A, Fernandez-Diaz L (1997) Nucleation, growth and zoning phenomena in crystallizing (Ba,Sr)CO3 Ba(SO4,CrO4, (Ba,Sr)SO4 and (Cd,Ca)CO3 solid solutions from aqueous solutions. *Geochimica et Cosmochimica Acta*, **61**, 3383–97.

Reeder R, Grams J (1987) Sector zoning in calcite cement crystals: implications for trace element distributions in carbonates. *Geochimica et Cosmochimica Acta*, **51**, 187–94.

Reeder R, Fagioli R, Meyers W (1990) Oscillatory zoning of Mn in solution-grown calcite crystals. *Earth-Science Reviews*, **29**, 39–46.

Rusk B, Reed M (2002) Scanning electron microscope-cathodoluminescence analysis of quartz reveals complex growth histories in veins from the Butte porphyry copper deposit, Montana. *Geology*, **30**, 727–30.

Rusk B, Reed M, Dilles J, Kent A (2006) Intensity of quartz cathodoluminescence and trace-element content in quartz from the porphyry copper deposit at Butte, Montana. *American Mineralogist*, **91**, 1300–12.

Rusk B, Lowers H, Reed M (2008) Trace elements in hydrothermal quartz: relationships to cathodoluminescent textures and insights into vein formation. *Geology*, **36**, 547–50.

Rye D, Bradbury H (1988) Fluid flow in the crust: an example from a Pyrenean thrust ramp. *American Journal of Science*, **288**, 197–235.

Shore M, Fowler A (1996) Oscillatory zoning in minerals: a common phenomenon. *The Canadian Mineralogist*, **34**, 1111–26.

Tesoriero A, Pankow J (1996) Solid solution partitioning of $Sr2^{+}$, $Ba2^{+}$, and $Cd2^{+}$ to calcite. *Geochimica et Cosmochimica Acta*, **60**, 1053–63.

Towell D, Winchester J, Spirn R (1965) Rare-earth distributions in some rocks and associated minerals of the batholith of southern California. *Journal of Geophysical Research*, **70**, 3485–96.

Uysal I, Zhao J, Golding S, Lawrence M, Glikson M, Collerson K (2007) Sm-Nd dating and rare-earth element tracing of calcite: implications for fluid-flow events in the Bowen Basin, Australia. *Chemical Geology*, **238**, 63–71.

Wang Y, Merino E (1992) Dynamic model of oscillatory zoning of trace elements in calcite: double layer, inhibition and self-organization. *Geochimica et Cosmochimica Acta*, **56**, 587–96.

Watson E (1996) Surface enrichment and trace-element uptake during crystal growth. *Geochimica et Cosmochimica Acta*, **60**, 5013–20.

Watson E (2004) A conceptual model for near-surface kinetic controls on the trace-element and stable isotope composition of abiogenic calcite crystals. *Geochimica et Cosmochimica Acta*, **68**, 1473–88.

Wogelius R, Fraser D, Wall G, Grime G (1997) Trace element and isotopic zonation in vein calcite from the Mendip Hills, UK, with spatial-process correlation analysis. *Geochimica et Cosmochimica Acta*, **61**, 2037–51.

Wood S (1990) The aqueous geochemistry of the rare-earth elements and yttrium; 2, theoretical predictions of speciation in hydrothermal solutions to 350°C at saturation water vapor pressure. *Chemical Geology*, **88**, 99–125.

Zhong S, Mucci A (1995) Partitioning of rare earth element (REEs) between calcite and seawater solutions at 25° and 1 atm, and high dissolved REE concentrations. *Geochimica et Cosmochimica Acta*, **59**, 443–53.